Towards Modelling AR Sco: Convergence to Aristotelian Electrodynamics and First Results

Louis Du Plessis

Supervisor: C. Venter
Collaborators: A.K. Harding
Z. Wadiasingh

Centre for Space Research, North-West University

October 2, 2024

AR Sco Observations

- Marsh et al. (2016) detected optical and radio pulsations from the binary white dwarf (WD) system AR Scorpii
- Orbital period of 3.55 hours and a “pulsar” spin period of 1.95 min
- Constrained the mass of the WD to $\sim 0.8 M_\odot$ and the M-dwarf companion to $\sim 0.3 M_\odot$
- Stiller et al. (2018) obtained a $\dot{P} = 7.18 \times 10^{-13}\ ss^{-1}$

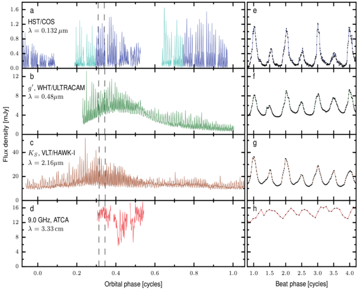

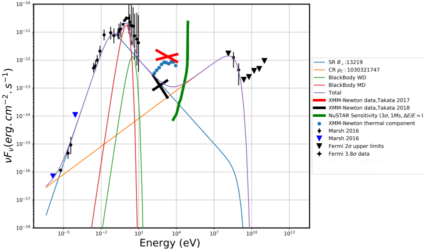

AR Sco Observations

- Optical and UV emission lines show no indication of an accretion disc
- The optical and UV are non-thermal emission and pulsed at the WD spin period
- This gives a light cylinder radius of $R_{\rm LC} = 5.6 \times 10^{11}$ cm and an orbital semi-major axis of $a = 8.5 \times 10^{10}$ cm
- Buckley et al. (2017) found that the system exhibits strong linear optical polarisation (up to $\sim 40\%$) and estimated the WD B-field to be $\sim 500\mathrm{MG}$

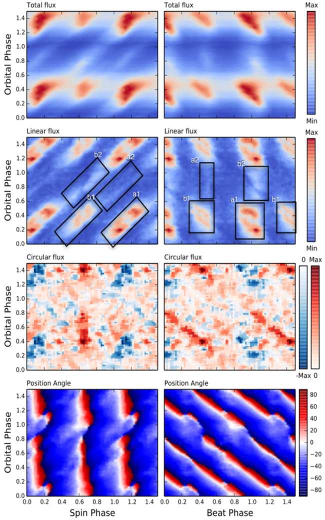

Figure: Optical data from Potter and Buckley (2018)

Aims

Develop a new general emission model to work for a WD binary scenario:

- Solve particle dynamics using the general equations of motion.
- Calculate the broadband light curves and spectra at different orbital phases.
-
- Calculate Stokes parameters, PPA, and degree of polarisation at different orbital phases.
- Calibrate our code with the pulsar emission code of Harding and collaborators.

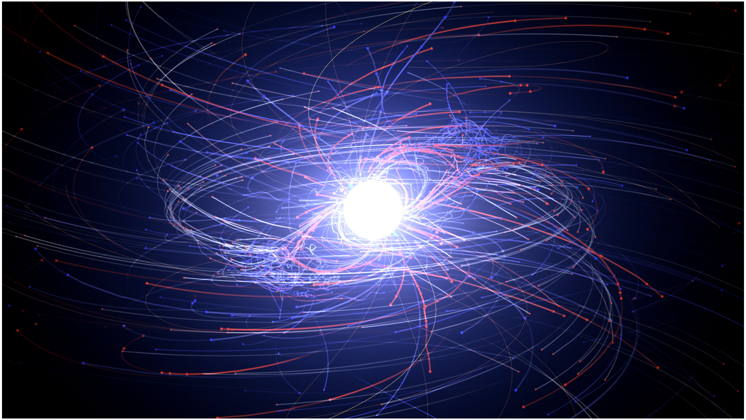

Adaptive ODE Solver

- Solve Lorentz equation:

$$\frac{d\mathbf{p}}{dt} = q\left(\mathbf{E} + \frac{c\mathbf{p}\times\mathbf{B}}{\sqrt{m^2c^4 + \mathbf{p}^2c^2}}\right). \quad (1)$$

- We investigated higher precision adaptive time step methods.

$$\Delta t_{n+1} = \Delta t_n \left(\frac{TOL}{T_{\mathrm{err}}}\right)^{-\frac{1}{kp}} \left(\frac{TOL}{T_{\mathrm{err;n-1}}}\right)^{-\frac{1}{kp}} \left(\frac{\Delta t_n}{\Delta t_{n-1}}\right)^{-\frac{1}{kp}}. \quad (2)$$

- Δt is the time step, TOL is the chosen tolerance for the truncation error T_{err}, p is the order of the chosen numerical method and $k = 8$.
- We used a limiting function to constrict the new time step.

$$\Delta t_l = \Delta t_n \left[1 + \kappa arctan\left(\frac{\Delta t_{n+1} - \Delta t_n}{\kappa\Delta t_n}\right)\right]. \quad (3)$$

- $\kappa \in [0.7, 2.0]$.

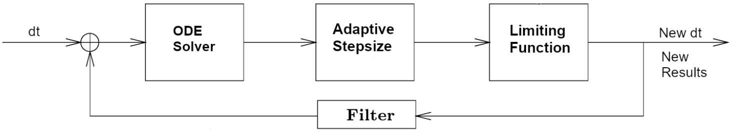

Calibration of ODE Solver

- Runge-Kutta Fehlberg 4(5): 5 stage.
- DVERK 6(5): 8 stage.
- Prince-Dormand 8(7): 12 stage.
- Adaptive Curtis 10(8): 18 stage.
- Adaptive Hiroshi 12(9): 29 stage.
- Vay Symplectic Scheme.

- Use test cases for high B-field, $E \times B$ (large $E_{\perp}$-fields), and RRF scenarios.
- Asses accuracy, stability, and computational time of each scheme to identify best scheme for our use case.

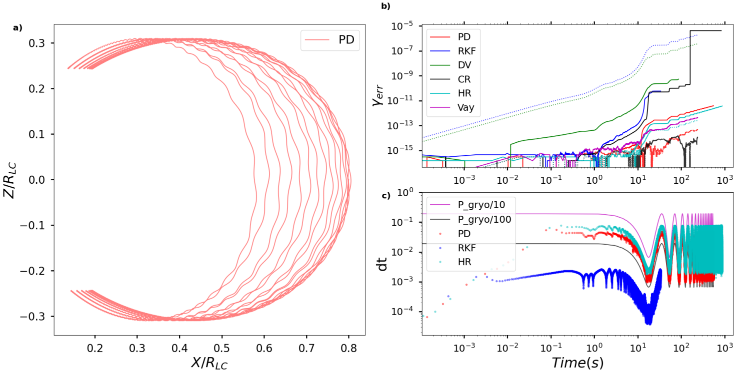

Radiation-Reaction Force

- Use equation from Landau and Lifshitz for general radiation-reaction force:

$$\begin{aligned}\mathbf{f} =& \frac{2e^3\gamma}{3mc^3}\left\{\left(\frac{\partial}{\partial t} + \mathbf{v}\cdot\nabla\right)\mathbf{E} + \frac{1}{c}\mathbf{v}\times\left(\frac{\partial}{\partial t} + \mathbf{v}\cdot\nabla\right)\mathbf{H}\right\} \\ &+ \frac{2e^4}{3m^2c^4}\left\{\mathbf{E}\times\mathbf{H} + \frac{1}{c}\mathbf{H}\times(\mathbf{H}\times\mathbf{v}) + \frac{1}{c}\mathbf{E}(\mathbf{v}\cdot\mathbf{E})\right\} \\ &- \frac{2e^4\gamma^2}{3m^2c^5}\mathbf{v}\left\{\left(\mathbf{E} + \frac{1}{c}\mathbf{v}\times\mathbf{H}\right)^2 - \frac{1}{c^2}(\mathbf{E}\cdot\mathbf{v})^2\right\}.\end{aligned} \tag{4}$$

- The first term is $\sim 10^8 - 10^{10}$ times smaller than the largest component.

$$E_{rad} = \int \mathbf{F}_{rad}\cdot\mathbf{v}.dt \tag{5}$$

- Benchmark Results:

Method	No-losses	RRF
RKF	1.0	1.7323
DV	0.4401	0.8565
PD	0.0706	0.1587
CV	0.0379	0.1259
HR	0.0529	0.1697

Pitch Angle Evolution

- Case a) $B = 10^8\,\mathrm{G}$, $E_\perp = 0.1B$,$\gamma_0 = 10^4$.
- Case b) $B = 10^{11}\,\mathrm{G}$, $E_\perp = 0.1B$,$\gamma_0 = 10^2$.
- Green: uniform $E \times B$ scenario.
- Cyan: uniform $E \times B$ with RRF scenario.
- Red: uniform B-field scenario.
- Blue: uniform B-field with RRF scenario.
- Panel a) no visible loss in θ_p due to RRF.
- Panel b) minor loss in θ_p due to RRF.
- SR cooling timescale has relative error of $10^{-4} - 10^{-3}$.

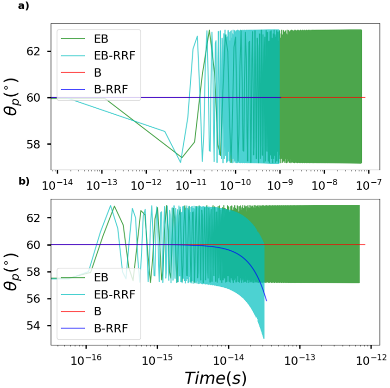

AE Results

- Aristotelian Electrodynamics velocity (gyro-centric):

$$\frac{\mathbf{v}_{AE}}{c} = \frac{\mathbf{E} \times \mathbf{B} \pm (B_0 \mathbf{B} + E_0 \mathbf{E})}{B^2 + E_0^2}. \quad (6)$$

- $\mathbf{E} \cdot \mathbf{B} = E_0 B_0$,
  $E^2 + B^2 = E_0^2 + B_0^2$.
- $F_{RRF} > F_L$ in observer frame but not particle frame.

$$\gamma_c = \left(\frac{3 E_0 R_c^2}{2|e|} \right)^{\frac{1}{4}}. \quad (7)$$

- θ_D is the angle between $\mathbf{v}$ and $\mathbf{v_{AE}}$.
- Convergence for the radiation reaction limited regime.
- $\theta_D \neq 0$ due to gyro-radius.
- See Du Plessis et al. (2024)

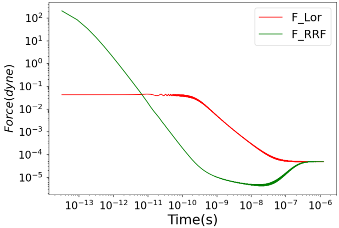

a)

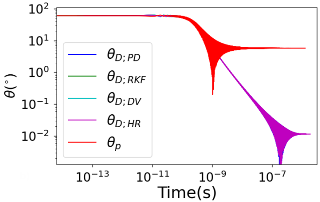

Harding and Collaborators' code

- Tracing out the particle trajectory incorporating $\mathbf{E} \times \mathbf{B}$ drift from Kalapotharakos et al. (2014).
- $\mathbf{v}/c = \mathbf{E} \times \mathbf{B}/(B^2 + E_0^2) + f\mathbf{B}/B$.
- Solving transport equations from Harding et al (2005) to calculate emission.
- $d\gamma/dt = eE_{\parallel}/mc - 2e^4B^2p_{\perp}^2/3m^3c^5$,
- $dp_{\perp}/dt = -3cp_{\perp}/2r - 2e^4B^2p_{\perp}^3/3m^3c^5\gamma$.
- For the Harding et al. 2015 and 2021 models these parameters are calculated with respect to the particle trajectory not the local B-field.

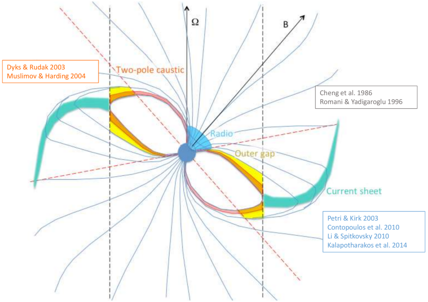

- These equations assume super relativistic particles with small pitch angles, gyrocentric trajectories, gyro-phase averaged trajectories an excludes drift effects.

Emission Map Calculations

- We calibrate with vacuum retarded dipole- and force-free fields.
- The phase corrections are given by:
- $\phi_{obs} = \phi_{em} - \mathbf{r}_{\mathbf{em}} \times \eta_{\mathbf{em}} / \mathbf{R}_{\mathbf{LC}} - \boldsymbol{\Delta}\phi_{\mathbf{rot}}$
- We use the same curvature- and synchrotron radiation calculations.
- Use $E_{\|}$-component to accelerate particle.

$$\rho_c = \frac{1}{\sqrt{(x'')^2 + (y'')^2 + (z'')^2}}. \quad (8)$$

- Figures from Barnard et al.(2022) for curvature radiation.

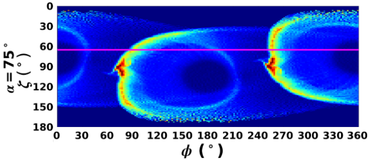

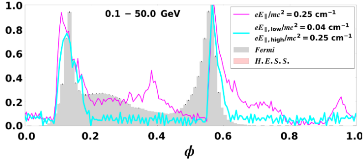

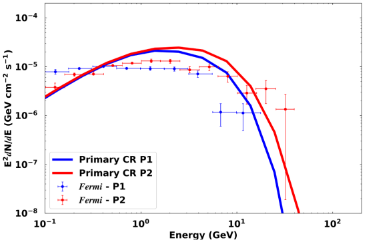

Divergence and Classical RRF

- B and E fields have 3 segments for the field structures:
- Vacuum-retarded dipole $R <= 0.2R_{LC}$.
- Force-free fields $0.4R_{LC} <= R$.
- Linear combination $0.2R_{LC} < R < 0.4R_{LC}$.
- FF coarse grids generated by Kalapotharakos et al. (2014) FIDO model.
- Test if $\nabla \cdot \mathbf{B} = 0$.
- Need to test if we are in the classical RRF regime:

$$E_{ex} = \frac{|\mathbf{p} \times \mathbf{B}|}{mc} \qquad (9)$$

- $E_{ex} < E_S$, where $E_S = 4.41 \times 10^{13}\,\mathrm{G}$.

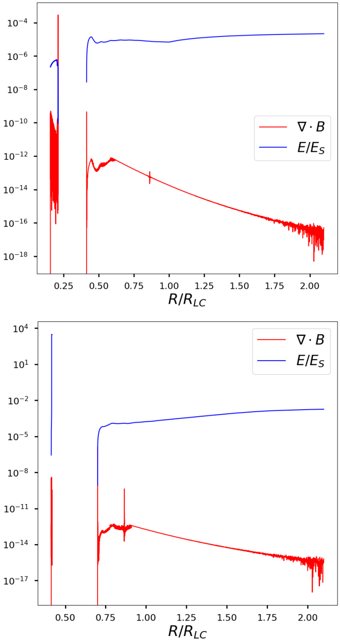

Force-Free Fields

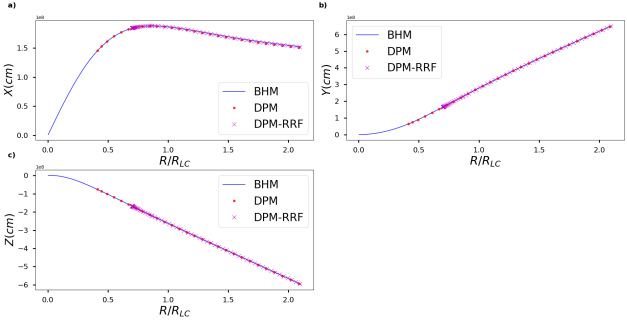

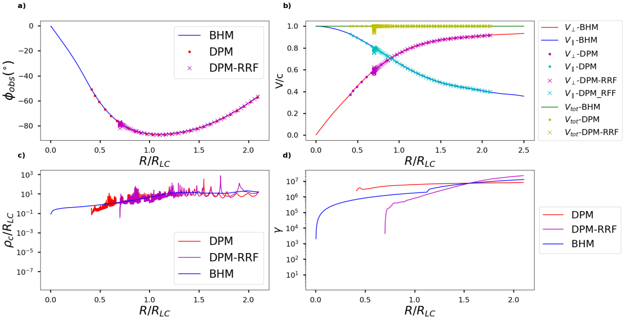

Emission Map Calculations

Skymaps and Spectra

- We first compare curvature radiation since it is least affected by the $E \times B$-drift for large $E_\perp$-fields.
- This is important since the traditional curvature, synchrotron and synchro-curvature radiation is derived by excluding an E-field.
- For initial comparison purposes we use their gyro-centric trajectory radius of curvature instead of our instantaneous radius of curvature of $\rho_e ff$.

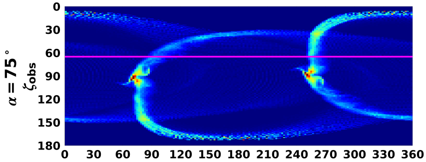

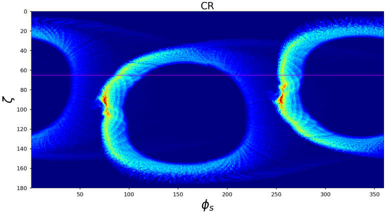

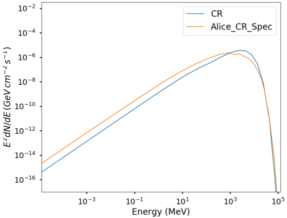

General Pitch Angle

- Discrepancy in pitch angle from Harding et al. (2021) trajectory and radiation transport equations.
- Quantum SR does keep θ_p small close to the surface but θ_p increases in the extended magnetosphere due to the $E \times B$-drift.
- Thus we need a general θ with respect to the $E \times B$ drifting trajectory to calculate the radiation.
- The assumption is that this trajectory is equivalent to AE thus we can assume the 'general pitch angle' as θ_D.
- Due to this changing 'general pitch angle' we also investigate the more general synchro-curvature radiation.

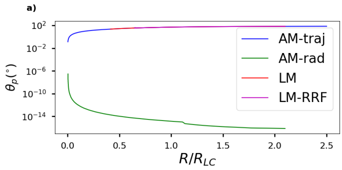

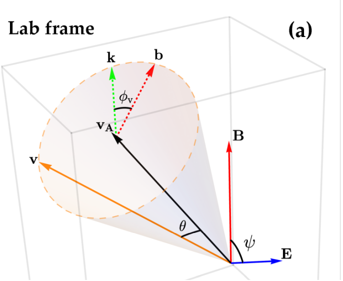

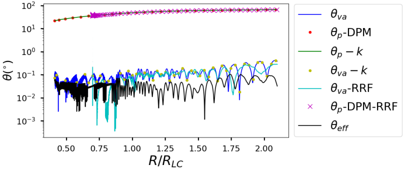

Synchrocurvature Radiation

- Kelner 2015, Cerutti 2016 synchrocurvature.

$$F_\nu(\nu) = \frac{\sqrt{3}e^3\overline{B}_\perp}{mc^2}\left(\frac{\nu}{\nu_c}\right)F(y) \quad (10)$$

- $\overline{B}_\perp = \sqrt{(\mathbf{E} + \beta \times \mathbf{B})^2 + (\beta \cdot \mathbf{E})^2}$.
- $\rho_{c;eff} = \gamma mc^2 / e\overline{B}_\perp$
- Vigano 2015 synchrocurvature (Harding et al. 2021).
- no E-field and standard θ_p.

$$F_\nu(\nu) = \frac{\sqrt{3}e^2\gamma y}{4\pi\hbar\rho_{eff}} \left[(1+z)F(y) - (1-z)K_{2/3}(y)\right]. \quad (11)$$

$$\rho_{c;eff} = \frac{\rho_c}{\cos^2\theta_p}\left(1 + \zeta + \frac{r_{gyr}}{\rho_c}\right)^{-1} \quad (12)$$

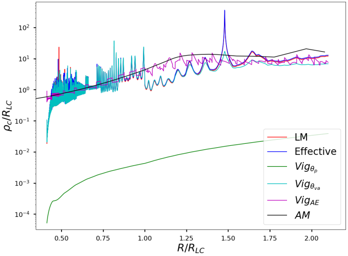

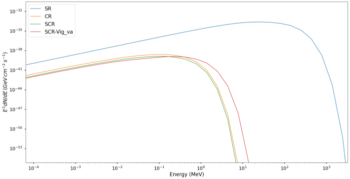

Emission Maps

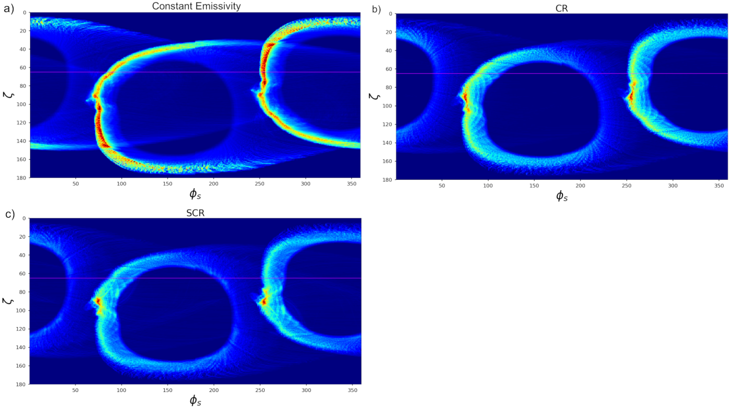

Results

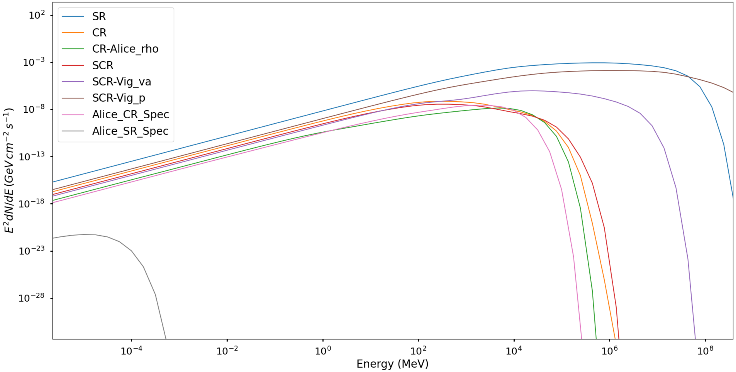

See Du Plessis et al. (2024; in prep)
See PhD Thesis to be uploaded to arXiv.

AR Sco Results

- Takata uses rewritten forms of equations from Harding et al. (2005).

$$\frac{d\gamma}{dt} = -\frac{P_\perp^2}{t_s}$$
$$\frac{d}{dt}\left(\frac{P_\perp^2}{B}\right) = -2\frac{B}{t_s\gamma}\left(\frac{P_\perp^2}{B}\right)^2 \tag{13}$$

- Where $t_s = 3m_e^3c^5/2e^4B^2$.
- $P_\perp = \gamma\beta\sin\theta_p$.
- These equations assume super relativistic particles with small pitch angles, gyro-phase averaged trajectories ,and exclude any particle drift effects.
- Using a static vacuum dipole our results agree reasonably well.
- Including an $E_\perp$-field there are many more mirrors.

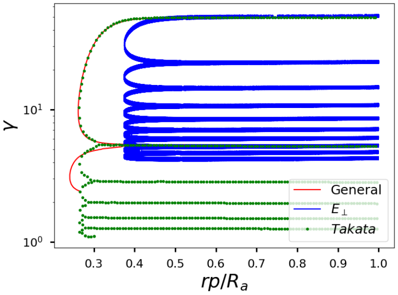

AR Sco Results

- Particles are injected into the WD magnetosphere at the companion.
- The particles are magnetically mirrored close to the WD surface where they are turned around.
- Particles given a standard power-law energy distribution $f(\gamma) = K_0\gamma^{-p}$.
- A uniform θ_p distribution is used to reproduce Takata et al. (2017).
- We only follow 1 field line.
- The WD $E_{\parallel}$-field is screened.
- We probed different WD B-field strengths, α-values, p-values and including and excluding the $E_{\perp}$-field.

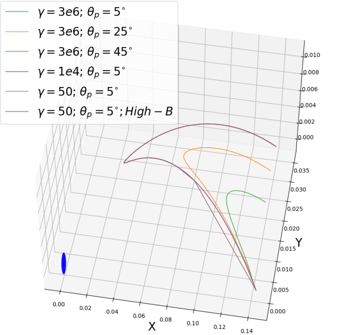

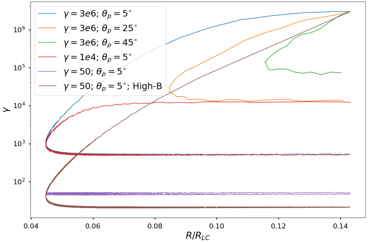

Emission Maps

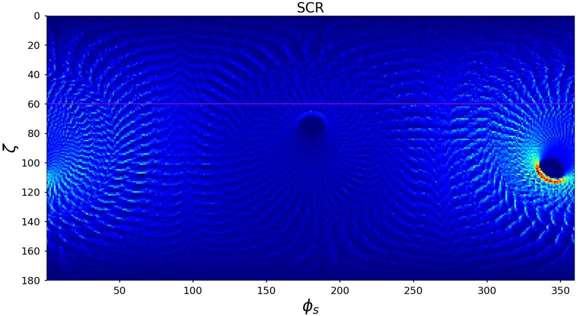

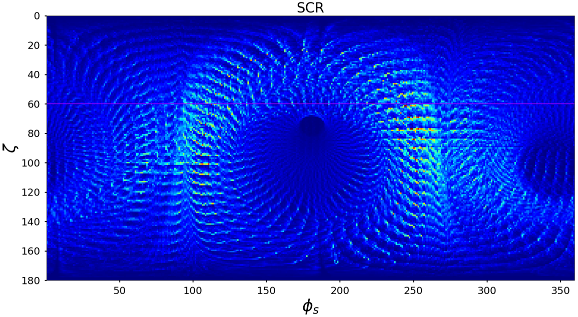

Spectra

- The Takata models use $\zeta = 60^\circ$, $\alpha = 60^\circ$, $B_S \sim 4 \times 10^8$ G, $\gamma_{min} = 50$, $\gamma_{max} = 3 \times 10^6$, excludes $E_\perp$, and $p = 2.5$ for their 2017 results and $p = 3.0$ for their 2019 results.
- For all our spectra we included $E_\perp$ except the specified case.

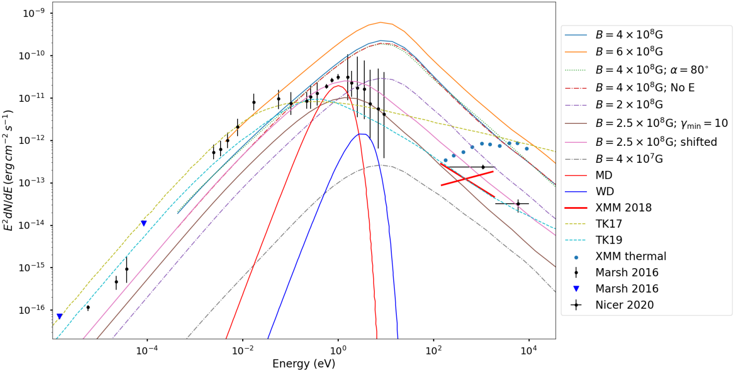

No $E_\perp$ Emission Maps

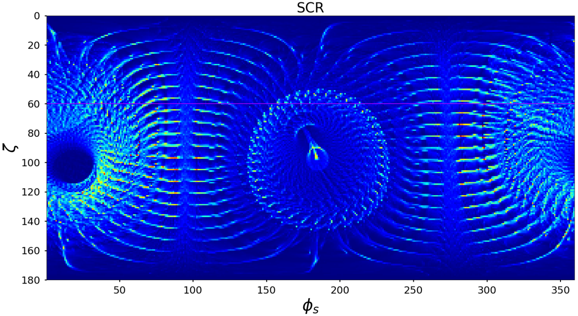

See Du Plessis et al. (2024/2025; in prep)
See PhD Thesis to be uploaded to arXiv.

Future Work

- October PhD Submission.
- Submit Calibration Paper.
- Constrain parameters better and do higher statistic runs with realistic pitch angle distribution for AR Sco results paper.
- Additional AR Sco modelling: Time dependant particle injection, build up orbital phase resolved emission maps, and probe different injection scenarios.
- Implement polarisation calculations to calculate Stokes parameters.
- Calculate fields self consistently to make code full PIC.
- Model other sources similar to AR Sco or that require general particle dynamics namely pulsars or intermediate polars.
- Improve computational cost of code: better adaptive time step method, SIMD operations, GPU processing.
- Calculate RRF for QED regime to test high field radiation-reaction limit close to the stellar surface in pulsars.

Bibliography

Buckley, D. A. H., Meintjes, P. J., Potter, S. B., Marsh, T. R., and Gänsicke, B. T. (2017). Polarimetric evidence of a white dwarf pulsar in the binary system AR Scorpii. *Nature Astronomy*, 1:0029.

Marsh, T. R., Gänsicke, B. T., Hümmerich, S., Hambsch, F.-J., Bernhard, K., Lloyd, C., Breedt, E., Stanway, E. R., Steeghs, D. T., Parsons, S. G., Toloza, O., Schreiber, M. R., Jonker, P. G., van Roestel, J., Kupfer, T., Pala, A. F., Dhillon, V. S., Hardy, L. K., Littlefair, S. P., Aungwerojwit, A., Arjyotha, S., Koester, D., Bochinski, J. J., Haswell, C. A., Frank, P., and Wheatley, P. J. (2016). A radio-pulsing white dwarf binary star. *Nature Astronomy*, 537:374–377.

Potter, S. B. and Buckley, D. A. H. (2018). Time series photopolarimetry and modeling of the white dwarf pulsar in AR Scorpii. *Mon. Not. Roy. Astron. Soc.*

Stiller, R. A., Littlefield, C., Garnavich, P., Wood, C., Hambsch, F.-J., and Myers, G. (2018). High-Time-Resolution Photometry of AR Scorpii: Confirmation of the White Dwarf's Spin-Down. *ArXiv e-prints*.